1999 International Mechanical Engineering Congress and Exposition (IMECE)
November 14-19, 1999, , Nashville, Tennessee
Invited Sessions on Control of Electro-hydraulic and fluid Systems

Design and Control of a Spherical Air Bearing System for multi-DOF Ball-joint-like Actuators

Kok-Meng Lee*, Dan E. Ezenekwe and Tian He***

*Georgia Institute of Technology, The George W. Woodruff School of Mechanical Engineering, Atlanta GA 30332-0405
**Corning Incorporated, Telecommunications Products Division, 14556 Highway 601 South, Midland, NC 28107

Abstract –This paper presents an analytical investigation on the design method and modeling of an air bearing system for ball-joint-like actuators. It addresses the method of regulating the three DOF translations of the rotor introduced by the air bearing system and thereby improving the dynamic performance of the orientation motion manipulation. The kinematics, which relates the rotor displacement and the air gaps, are essential for design optimization, dynamic simulation and motion control, are derived in closed-form. With a detailed modeling of the pressure-flow relationship as a function of the rotor position, the forces and dynamics of the system are formulated, and design methods of regulating the rotor displacement have been explored analytically. Simulation results suggest that the fluid forces could be generated to passively stabilize the otherwise open loop unstable electromagnetic system. It is expected that this research will be a basis for designing and evaluating an improved VR spherical motor with enhanced torque capability by eliminating mechanical friction.

1. INTRODUCTION

Many applications in the industry require the use of fluid bearings to overcome friction, provide more precise location and alignment of components, and enable smooth movement of large components from one point to another point. In other applications, precision alignment of parts is very critical to the quality and specifications of the product. As advances in technology continue to demand more accurate and precision devices, there are opportunities to utilize the unique attractive features of air bearing systems to meet these challenges.

We explore the use of a non-contact, spherical air bearing system for multi-DOF spherical actuators [1] which operates on the principles of variable reluctance (VR). The motor combines the roll, pitch, yaw motion in one joint making it attractive for many applications. Besides the capability of three degree-of-freedom (DOF) motions in one joint, the motor has large range of motion, isotropic properties and no singularities within the workspace. These flexible design features make the VR spherical motor suitable for a wide range of applications such as water-jet cutting, laser cutting, painting, welding, material handling, coordinate measurement etc., where smooth uniform manipulation of the end-effector is required.

Three basic techniques used in non-contact bearing designs; namely, fluid bearing, magnetic levitation, and the Meissner effect. Non-contact air bearing is considered here since it has the potential to enhance the motor performance for more advanced applications, has cooling effect on interacting components and does not interfere with actuator electromagnetic system. Many researchers [2] [3] have investigated bearing designs and characteristics. Other authors [4] [5] [6] have contributed to improving bearing stability of fixed orifices and. Recently, there has been some work on control of air-bearing devices [8]. These works have concentrated on single axis bearing devices. In this paper we are interested in the control of multi-DOF spherical devices.

The reminder of this paper is organized as follows: The next section discusses the bearing design configuration for a ball-joint-like spherical device. This is followed by the characterization of airflow through the bearing in Section 3, which generates the forces on the rotor. Then, the system dynamics is presented in Section 4 and followed by design methodology and simulations in Section 5. Finally, a conclusion is presented.

2. BEARING FOR BALL-JOINT-LIKE DEVICES

Consider an arbitrary displacement of the two spherical surfaces as shown in Figure 1, where $\vec{r}_o$ is the rotor displacement with respect to the center of the stator.

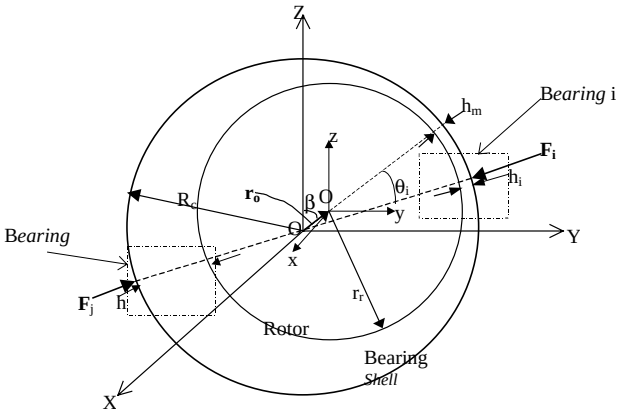

Figure 1 Conceptual schematics illustrating spherical bearing

In Figure 1, the reference frame *XYZ* is defined at the center of the stator, *O*, with the *Z*-axis pointing towards the opening for the stator and *xyz* is fixed at the center of the rotor, *O'*, with its z-axis along the rotor output shaft. At equilibrium, the coordinate frames *XYZ* and *xyz* have a common origin at their centers. Thus, any position on the rotor can be expressed with respect to the *XYZ* coordinate system using a 4X4 homogeneous transformation matrix, [*T*]:

$$[P]_{XYZ} = [T][P]_{xyz} \quad (1)$$

where $[P]_{XYZ}$ and $[P]_{xyz}$ are the position of a point on the rotor measured with respect to XYZ and *xyz* respectively.

2.1 Bearing Configurations

The design concept is to use pressurized air to regulate the rotor such as the rotor displacement $\vec{r}_o$ is null regardless of any "disturbances" caused by the electromagnetic actuation or an external force. Multiple independent spherical bearings are strategically designed to support the rotor. In general, the more the number of bearings, the larger the load the system is capable of supporting. The challenge, however, is to design a compact yet efficient air bearing system to fit into the limited surface area of the rotor. In addition, the bearings should be designed so that they do not interfere with the electromagnetic poles of the spherical motor, which are located following the pattern of a regular polygon.

Theoretically, the minimum number of non-coplanar forces required to achieve bi-directional position control of the spherical rotor in a three-dimensional space is four. One possible arrangement of a minimum number of bearings is to place the bearings at locations corresponding to the vertices of a regular tetrahedron. The arrangement of minimum number of bearings is not necessarily attractive since four independent actuators are required, and that the four point bearings can not be grouped in pairs such that the couples exert equal and opposite forces along their lines of action.

An attractive alternative is to design so that pressurized air passes through its center enabling the unit to serve as a bearing. The advantages of joint magnetic-pole/bearing units are twofold: (1) The air jet will provide cooling effect to the coil windings. (2) It will optimize the stator surface by maximizing the size of a bearing, thereby enhancing load-bearing capacity. In the following discussion, we shall consider the case where six or more bearing points are evenly spaced on the spherical bearing such that bearing forces can always be grouped in pairs. As illustrated in Figure 1, the pair of bearing forces $\vec{F}_i$ and $\vec{F}_j$ exert equal but opposite forces through the center of the stator.

2.2 Forward Kinematics

The gap between the stator and rotor along a pair of forces, $\vec{F}_i$ and $\vec{F}_j$, can be determined with the aid of Figure 2. The net force, $\vec{F}_{ij} = \vec{F}_i + \vec{F}_j$, can be described by:

$$\vec{F}_{ij} = F_{ij}\vec{e}_{ij} \quad (2)$$

where F_{ij} and $\vec{e}_{ij}$ are the magnitude and the unit vector (known) of the resultant force. As shown graphically in Figure 2b, the minimum air gap between the rotor and the stator is in the direction of $\vec{r}_o$. Thus, the included angle between $\vec{F}_{ij}$ and $\vec{r}_o$ is

$$\theta_{ij} = \cos^{-1}(\vec{e}_{ij} \cdot \vec{e}_{ro}) = \cos^{-1}\left(\frac{\vec{F}_{ij} \cdot \vec{r}_o}{F_{ij}\, r_o}\right) \quad (3)$$

where r_o is the magnitude and $\vec{e}_{ro}$ is the unit vector of $\vec{r}_o$. For a given rotor displacement, the air gaps, $h_{i,}$ and h_j are given by Equations (4a) and (4b):

$$h_i = r_s - \left\{\sqrt{r_r^2 - r_o^2 \sin^2\theta_{ji}} + r_o \cos\theta_{ji}\right\} \quad (4a)$$

and

$$h_j = r_s - \left\{\sqrt{r_r^2 - r_o^2 \sin^2\theta_{ji}} - r_o \cos\theta_{ji}\right\} \quad (4b)$$

where r_s and r_r are the radii of the stator and rotor at the interface respectively.

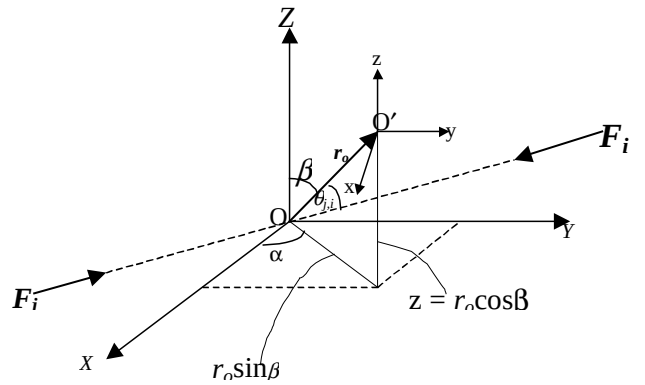

(a) Rotor displacement

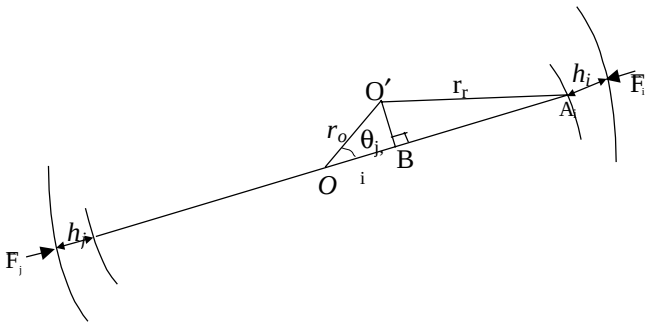

(b) Bearing force line of action

Figure 2 Schematics for gap determination

2.3 Inverse Kinematics

Since direct sensing of the rotor displacement $\vec{r}_o$ is difficult, the inverse kinematics provides a practical means of computing the rotor position from the air gaps measurements. With three independent pairs of gap

measurements, the three orthogonal components of the rotor displacement can be determined as follows.

Subtracting Equation (4a) from Equation (4b), we have

$$r_o \cos\theta_{ji} = \vec{r}_o \cdot \vec{e}_{j,i} = \frac{h_j - h_i}{2} \tag{5a}$$

Two other similar equations can be obtained from two other pairs of bearing forces.

$$\vec{r}_o \cdot \vec{e}_{j-1,i-1} = \frac{h_{j-1} - h_{i-1}}{2} \tag{5b}$$

$$\vec{r}_o \cdot \vec{e}_{j+1,i+1} = \frac{h_{j+1} - h_{i+1}}{2} \tag{5c}$$

Equations (5a), (5b), and (5c) can be written in matrix form:

$$\begin{bmatrix} \vec{e}_{j-1,i-1} & \vec{e}_{j,i} & \vec{e}_{j+1,i+1} \end{bmatrix} \begin{bmatrix} r_x \\ r_y \\ r_z \end{bmatrix} = \frac{1}{2} \begin{bmatrix} h_{j-1} - h_{i-1} \\ h_j - h_i \\ h_{j+1} - h_{i+1} \end{bmatrix} \tag{6}$$

where r_x, r_y *and* r_z are the components of $\vec{r}_o$ in the direction of X, Y and Z respectively.

3. AIR BEARING DYNAMIC MODEL

Figure 3 shows a schematic of a simple, pocketed, orifice compensated bearing. Air enters from a pressure source, passes through an orifice restriction of diameter d_o, then expands isentropically into the pocket of diameter R_p and recess d_p, and finally exhausts to the atmosphere through the annulus which consists of two parallel surfaces of spacing h.

3.1 Flow characteristics

The following assumptions are made in deriving the dynamic model: (1) The pressure in the pocket is uniform. (2) The air is isothermal. (3) Changes in air density are attributed mainly to variations in pressure and the ideal gas law, $p = \rho RT$ where p, R and T are the pressure, gas constant and temperature of the air respectively, is assumed to hold throughout. Thus, the force acting on the rotor is given by integrating the pressure over the bearing surface as follows:

$$f = 2\pi \left[\int_0^{R_p} p_p r dr + \int_{R_b}^{R_b} p r dr \right] \tag{7}$$

where p_p and p are the pressures in the pocket and the annulus respectively. The mass m contained in the bearing is a function of the rotor displacement along the direction of the actuating force as well as the air density and the state of the air. The time rate of change of the air is the difference between the inflow and the outflow, or

$$\frac{dm}{dt} = q_R - q_o \tag{8}$$

where m is the mass of the air contained between the bearing surfaces; and q_R and q_o are the mass flow rate through the orifice restriction and the exhaust respectively. The mass m is given by

$$m = 2\pi \left[\int_0^{R_p} (d_p + h) \rho r dr + \int_{R_p}^{R_b} h \rho r dr \right]$$

or

$$m = \frac{p_p}{RT} \pi R_p^2 (d_p + h) + \frac{2\pi}{RT} \int_{R_p}^{R_b} hp r dr \tag{9}$$

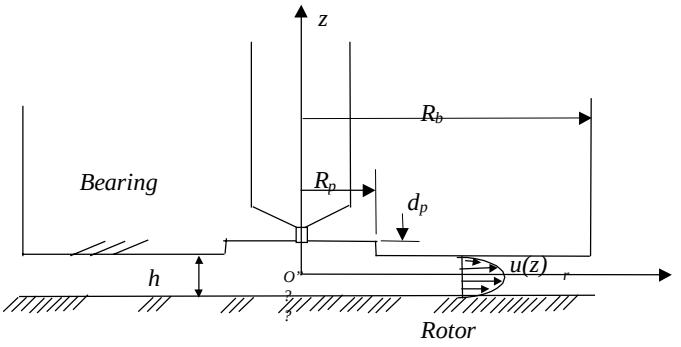

Figure 3 Orifice compensated air bearing

Since the gap in the annulus is very small and the pressure variation in the z-direction is negligible, the flow between the surfaces is laminar. Thus, the flow-pressure relationship through the annulus, which is essentially laminar flow between two parallel surfaces, can be shown to be

$$p^2 = p_a^2 + \frac{12\mu q_o RT}{\pi h^3} \ln\left(\frac{R_b}{r}\right)$$

which can be re-arranged for the flow rate as a function of pressure and the air gap follows:

$$q_o = \frac{(p_p^2 - p_a^2)\pi h^3}{12\mu RT \ln\left(\frac{R_b}{R_p}\right)} \tag{10}$$

The flow through an orifice has been modeled by several authors [8]. A particular form known as Fliegner's approximation [9] has been chosen for this analysis due to its convenience for analytical and computational purposes.

$$q_R = 2\left(\frac{\pi d_o^2}{4}\right)\left[\frac{\gamma}{RT}\left(\frac{2}{\gamma+1}\right)^{\frac{\gamma+1}{\gamma-1}}\left(p_s p_p - p_p^2\right)\right]^{\frac{1}{2}} \tag{11}$$

3.2 Perturbation model

Note that the flow-pressure relationships given by Equations (10) and (11) are highly non-linear. For the study of the dynamics due to a small deviation of the rotor displacement about the equilibrium as shown in Figure 2b, a perturbation model about an equilibrium operating condition (where the rotor is concentric with the stator), is derived. For this purpose, the pressure in the annulus is approximated by a linear relationship as follows:

$$p = p_p - (p_p - p_a)\frac{r - R_p}{R_b - R_p} \tag{12}$$

where the subscript 'e' denotes the variables are evaluated at the steady state. The total force acting on the rotor is obtained by integrating the pressure over the bearing surfaces.

$$\tilde{f} = 2\pi\left[\int_0^{R_p}(\tilde{p}_{pi} - \tilde{p}_{pj})rdr - \int_{R_p}^{R_b}(\tilde{p}_{pi} - \tilde{p}_{pj})\frac{r - R_p}{R_b - R_p}rdr\right] \tag{13}$$

where the first integrand is at the pocket and the second is from the bearing annulus; the ~ sign denotes variation from equilibrium values.

$$\tilde{f} = \tilde{p}_p A_{eq} \tag{14}$$

where $\tilde{p}_p = \tilde{p}_{pi} - \tilde{p}_{pj}$

and $A_{eq} = \pi R_{eq}^2 = \frac{\pi}{3}(R_b^2 + R_b R_p + R_p^2)$.

In Equation (14), the deviation of the pocket pressure p_p depends on the flow-pressure characteristics of the bearing. Since there is no contact between the surfaces and frictional effect of air is negligible, the equation of motion for the rotor along the direction of the actuating force is

$$m_r \ddot{\tilde{h}}_i = A_{eq}\tilde{p}_p . \tag{15}$$

At equilibrium, since the gap h is equal to h_e and there is no change of air stored in the bearing, the flow through the orifice is equal to that through the annulus, q_e. To the first degree of Taylor series approximation, the small deviation of the flow rate through the restrictor about the equilibrium can be written as

$$\tilde{q}_R = -a_1\tilde{p}_p + a_2\tilde{p}_s \tag{16}$$

where $\tilde{p}_s = \tilde{p}_{si} - \tilde{p}_{sj}$; $\tilde{q}_R = \tilde{q}_{ri} - \tilde{q}_{Rj}$; and

$$a_1 = \left.\left(\frac{\partial(q_R)}{\partial p_p}\right)\right|_{\substack{p_p = p_{pe} \\ q_R = q_e}} = \frac{q_e}{2p_s}\left(\frac{2 - \frac{p_s}{p_{pe}}}{\frac{p_s}{p_{pe}} - 1}\right)$$

$$a_2 = \left.\left(\frac{\partial q_R}{\partial p_s}\right)\right|_{\substack{q_R = q_e \\ p_p = p_{pe}}} = \frac{q_e}{p_s - p_{pe}}$$

The corresponding linear approximation of the flow rate through the annulus about the equilibrium condition can be derived from Equation (10b), which yield

$$\tilde{q}_o = a_3\tilde{p}_p + a_4\tilde{h}_i \tag{17}$$

$$a_3 = \left.\frac{\partial(q_o)}{\partial p_p}\right|_{\substack{q_o = q_e \\ p_p = p_{pe}}} = \frac{2q_e p_{pe}}{(p_p^2 - p_a^2)}$$

$$a_4 = \left.\left(\frac{\partial(q_o)}{\partial h_i}\right)\right|_{h_i = h_e} = \frac{3q_e}{h_e}$$

where $\tilde{q}_o = \tilde{q}_{oi} - \tilde{q}_{oj}$ and note that $\tilde{h}_j = -\tilde{h}_i$.

As shown in Equation (8), the difference between the flow through the restriction and the annulus is stored in the bearing. Substituting p from Equation (12) into Equation (9), we have

$$m = \frac{[h_i p_p A_{eq} + d_p\ p_p \pi R_p^2 + h_i p_a(\pi R_b^2 - A_{eq})]}{RT} \tag{18}$$

the linear approximation of which is given as follows:

$$\frac{d\tilde{m}}{dt} = a_5\dot{\tilde{p}}_p + a_6\dot{\tilde{h}} \tag{19}$$

where $a_5 = \left.\left(\frac{\partial m}{\partial p_p}\right)\right|_e = \frac{A_{eq}h_e + d_p\pi R_p^2}{RT}$

$$a_6 = \left.\left(\frac{\partial m}{\partial h_i}\right)\right|_e = \frac{A_{eq}(p_{pe} - p_a) + \pi R_b^2 p_a}{RT} .$$

Hence,

$$a_5\dot{\tilde{p}}_p + a_6\dot{\tilde{h}}_i = (-a_1\tilde{p}_p + a_2\tilde{p}_s) - (a_3\tilde{p}_p + a_4\tilde{h}_i) \tag{20}$$

To obtain a dynamic equation in term of h_i explicitly, we eliminate the pressure p_p by substituting it and its time derivative from Equation (15) into Equation (20). The resulting equation of the rotor motion is given by

$$\dddot{\tilde{h}}_i + \left(\frac{a_1 + a_3}{a_5}\right)\ddot{\tilde{h}}_i + \left(\frac{A_{eq}a_6}{a_5 m_r}\right)\dot{\tilde{h}}_i + \left(\frac{A_{eq}a_4}{a_5 m_r}\right)\tilde{h}_i = \left(\frac{A_{eq}a_2}{a_5 m_r}\right)\tilde{p}_s \tag{21}$$

Using Routh Hurwitz stability criteria, the condition for an asymptotically stable system implies $\frac{(a_1 + a_3)a_6}{a_4 a_5} > 1$, which yields $\frac{1}{3}\left[\frac{\frac{3}{2}p_s - p_{pe}}{p_s - p_{pe}}\right] > 1$ or $p_{pe} > \frac{3}{4}p_s$. In addition, all the coefficients must be positive for stability implies that $p_{pe} < p_s$. Hence,

$$\tfrac{3}{4}p_s < p_{pe} < p_s . \tag{22}$$

4. DESIGN METHODOLOGY

Consider the case where the supply pressure is constant ($\tilde{p}_s = 0$). In order words, the air bearing system is essentially a passive regulator.

4.1 Design Tradeoff's

Note that the system is third-order and thus at least one of the characteristic roots is real which implies that Equation (21) can be written in the following form:

$$(s+\sigma)(s^2+2\xi\omega_n s+\omega_n^2)=0 \tag{23}$$

By expanding Equation (23) and equating its coefficients that the corresponding terms in Equation (21), the design parameters (σ, ξ and ω_n) can be related to the system parameters as follows:

$$\sigma+2\xi\omega_n=\frac{C_2}{\left(1+C_a\frac{d_p}{h_e}\right)}\frac{q_e}{h_e} \tag{23a}$$

$$\omega_n^2+2\xi\omega_n\sigma=\frac{C_1}{h_e\left(1+C_a\frac{d_p}{h_e}\right)} \tag{23b}$$

$$\sigma\omega_n^2=\frac{C_o}{\left(1+C_a\frac{d_p}{h_e}\right)}\frac{q_e}{h_e^2} \tag{23c}$$

where

$$C_2=\frac{RT}{A_{eq}}\left[\frac{2p_{pe}-p_s}{2p_{pe}(p_s-p_{pe})}+\frac{2p_{pe}}{p_{pe}^2-p_a^2}\right] \tag{24a}$$

$$C_1=\frac{A_{eq}(p_{pe}-p_a)+\pi R_b^2 p_a}{m_r} \tag{24b}$$

$$C_o=\frac{3RT}{m_r} \tag{24c}$$

$$C_a=\frac{\pi R_p^2}{A_{eq}} \tag{24d}$$

Note that A_{eq} is generally constrained by the spherical actuator geometry. Thus, Equations (23a), (23b) and (23c) represent the design trade-off's among the three design variables, q_e, h_e, and d_p for a specified dynamic response, which can be expressed as

$$q_e=\frac{1+n}{1+4n\xi^2}\frac{C_1}{C_2\omega_n} \tag{26}$$

$$h_e=\frac{1+n}{n}\frac{C_o}{C_2\omega_n^2} \tag{27}$$

$$d_p=\frac{C_o}{C_aC_2\omega_n^2}\left(\frac{C_1C_2}{C_o}\frac{1}{1+4n\xi^2}-\frac{n+1}{n}\right) \tag{28}$$

where $n=\frac{2\xi\omega_n}{\sigma}$. The effect of the third pole could be reduced if σ is large compared to $\xi\omega_n$ (or n>>1). However, for a practical air bearing system, the pocket depth must be real, finite and positive and thus imposes a constraint on the choice of ω_n, σ, and ξ.

4.2 Design Example

Table 1 lists the parameters determined for the spherical motor [1] where the stator poles are located following the pattern of an Icosahedron.

Table 1: Parameters

Parameters	Value
Mass m_r, (kg)	0.2
Outer radius R_b, (mm)	12.7
R_b/R_p	16
Supply pressure, p_s (KN/m^2)	420
P_{pe}/p_s	0.92

Figures 4(a) and (b) show the pocket depth plotted as a function of natural frequency and damping ratio respectively. As h_e, and d_p are inversely proportional to ω_n^2, we chose ω_n*=240 Hz* (or 1,508rad/sec), $\sigma=2\xi\omega_n$ (or *n=1*) and ξ*=0.5* to provide a reasonable physical size for the pocket depth and the air gap and acceptable dynamic response. The corresponding calculated parameters are q_e = 1.281e-5 Kg/s, h_e = 0.069mm and d_p = 0.019mm.

The air bearing and electromagnetic system are simulated using MATLAB for two cases. The first case is one degree-of-freedom with only a pair of bearings. Figures 5(a) and (b) shows the rotor displacement in the direction of actuating force for an initial displacement of 5.8μm respectively. Although the electromagnetic system is open-loop unstable, the air bearing system is shown to dominate the magnetic system and stabilizes the combined system.

The second case is a three degree-of-freedom with five pairs of bearings located on ten of the stator poles without the top and bottom vertices of the Icosahedron. The 3-D simulation discussed below computes the displacement, velocity and acceleration vectors for multiple bearings (5 pairs) and decomposes them into the orthogonal directions. Since each air bearing system is linear, we compute the resultant forces on the rotor dynamics in 3-D by using vectors to sum the individual contributions.

5. CONCLUSIONS

We have presented the method for design of a practical air bearing system for a VR spherical motor. Specifically, this paper addresses the following fundamental issues of the bearing system design:

(1) The method of generating the necessary rotor support forces with externally pressurized air and the strategic arrangement of point bearings is discussed.

(2) The forward and inverse kinematics between the rotor displacement and the individual air gaps at positions round the stator are developed in closed-forms, which are essential for design, dynamic simulation and control purposes.

(3) Along with the pressure-flow relationship as a function of the rotor position, the paper presents a detailed dynamic model of the air bearing. Trade-off's between the design parameters and the dynamic performance of the air bearing regulator system have been discussed with using a design example.

The studies have led to the design of a potentially useful air-bearing system capable of eliminating frictions in ball-joint-like actuators. The dynamic performance of the air bearing system has been evaluated analytically by simulation.

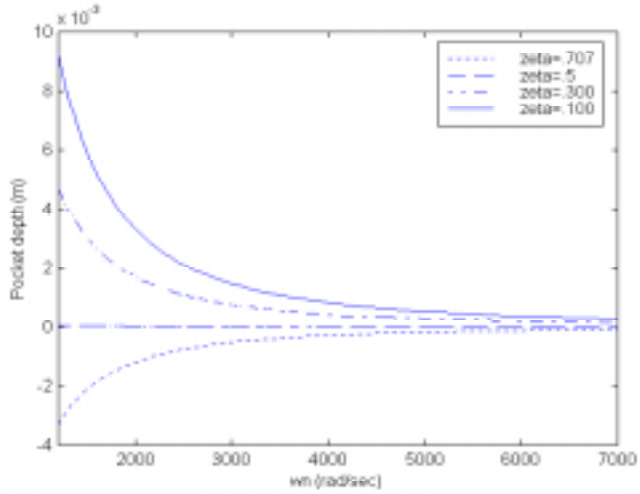

(a) Pocket depth Vs natural frequency ($n = 1$)

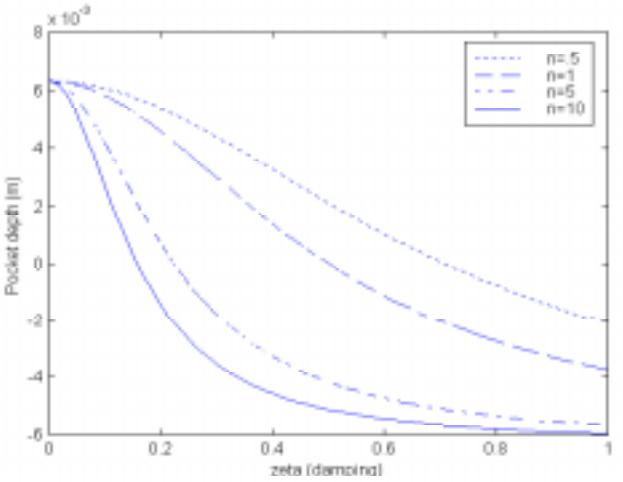

(b) Pocket depth Vs damping ratio ($\omega_n = 240\ Hz$)

Figure 4 Effect of ω_n and ξ on the choice of pocket depth

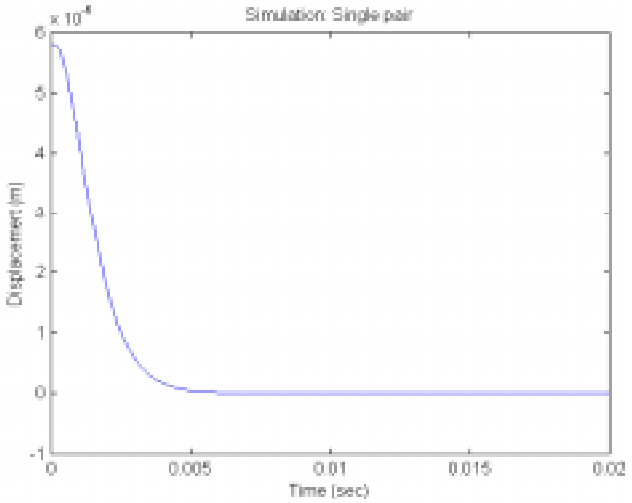

(a) Rotor displcement (1-DOF)

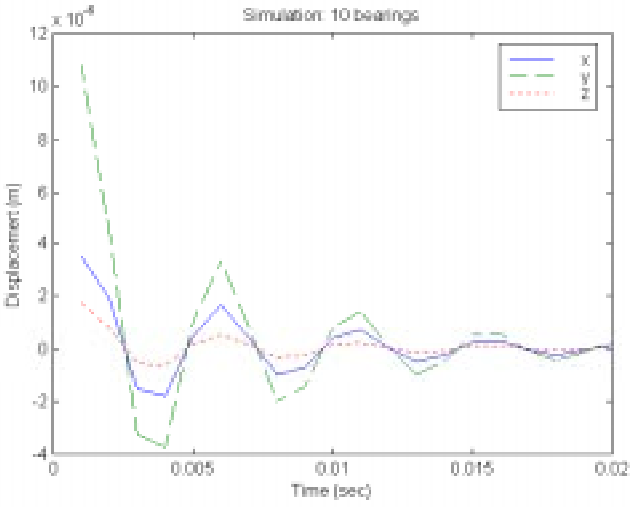

(b) Rotor displcement (3-DOF)

Figure 5 Simultion results of rotor displacement

REFERENCES

[1] Lee, K.-M., Roth, R., and Zhou, Z., "Dynamic Modeling And Control Of A Ball-Joint-Like Variable Reluctance Spherical Motor," ASME Journal Of Dynamics Systems, Measurements, And Control, Vol. 118, No. 1, March 1996, pp.29-40.

[2] Fearing, R. S., "Micro Structures and Micro Actuators for Implementing Sub-millimeter Robots," excerpts from Precision, Sensors, Actuators and System, Kluwer Academic Publishers, Netherlands, 1990, pp. 39-72.

[3] Hamcock, B. J., "Fundamentals of Fluid Film Lubrication," McGraw-Hill Inc., NY, 1994.

[4] Licht, L., Elrod, H., "A Study of the Stability of Externally Pressurized Gas Bearings", ASME Journal of Applied Mechanics, Vol. 82, 1960, pp. 250-258.

[5] Mori, H., Mori, A. Kaneko, R., Yoshida, K., "Stability Element for External Pressurized Gas Bearing (2nd Report, Stabilizing Element Inserted into the Gas Supply Line)", Transactions of JSME, Vol. 32, No. 244, 1966, pp. 1883-2064.

[6] Ohsumi, T., Ikeuchi, K., Mori, H., Haruyama, H. J., Matsumoto, Y., "Characteristics of a Hydrostatic Bearing with a Controlled Compensating Element", Wear, Vol. 105, April, 1991, pp. 177-194.

[7] Sato, Y., Murata, K., Harada, M., "Dynamic Characteristics of Hydrostatic Thrust Air Bearing with Actively Controlled Restrictors", Transactions of ASME (tribology Conf.), Vol. 110, No. 1, Jan., 1988, pp. 156-161.

[8] Licht, L., Fuller, D. D., Sternlicht, B., "Self-Excited Vibrations of an Air-Lubricated Thrust Bearing", Transactions of ASME, Vol. 80, 1958, pp.411-414.

[9] Slocum A. H., "Precision Machine Design", Prentice-Hall Englewood Cliffs, NJ, 1992.